PRIFYSGOL BANGOR / BANGOR UNIVERSITY

PRIFYSGOL
BANGOR
UNIVERSITY

Effect of polarization sensitivity on ultrasmall SOI-based AWG for FBG sensor interrogation

Li, Hongqiang; Xie, Rui; Hong, Yanhua; Zhang, Zanyun; Zhang, Cheng; Tang, Chunxiao; Li, Enbang

Optical Engineering

DOI:
10.1117/1.OE.57.6.065103

Published: 27/06/2018

Peer reviewed version

Cyswllt i'r cyhoeddiad / Link to publication

Dyfyniad o'r fersiwn a gyhoeddwyd / Citation for published version (APA):
Li, H., Xie, R., Hong, Y., Zhang, Z., Zhang, C., Tang, C., & Li, E. (2018). Effect of polarization sensitivity on ultrasmall SOI-based AWG for FBG sensor interrogation. *Optical Engineering*, *57*(6). https://doi.org/10.1117/1.OE.57.6.065103

Hawliau Cyffredinol / General rights
Copyright and moral rights for the publications made accessible in the public portal are retained by the authors and/or other copyright owners and it is a condition of accessing publications that users recognise and abide by the legal requirements associated with these rights.

• Users may download and print one copy of any publication from the public portal for the purpose of private study or research.
• You may not further distribute the material or use it for any profit-making activity or commercial gain
• You may freely distribute the URL identifying the publication in the public portal ?

Take down policy
If you believe that this document breaches copyright please contact us providing details, and we will remove access to the work immediately and investigate your claim.

05. May. 2023

Effect of polarization sensitivity on ultrasmall SOI-based AWG for FBG sensor interrogation

Hongqiang Li[a,*], Rui Xie[a], Yanhua Hong[b], Zanyun Zhang[a], Cheng Zhang[a], Chunxiao Tang[a], Enbang Li[c]

[a]Tianjin Key Laboratory of Optoelectronic Detection Technology and Systems, School of Electronics and Information Engineering, Tianjin Polytechnic University, Tianjin 300387, China
[b]School of Electronic Engineering, Bangor University, Bangor LL57 1UT, U.K.
[c]School of Physics, University of Wollongong, Wollongong, NSW 2522, Australia

Abstract. Polarization sensitivity is an important factor that affects the interrogation of ultrasmall arrayed waveguide grating (AWG) for fiber Bragg grating (FBG) sensor. An ultrasmall 1×8 silicon-on-insulator (SOI) AWG with a core size of less than $530\mu m \times 480\mu m$ is proposed in this study. This ultrasmall SOI AWG exhibits good transmission spectra and high polarization sensitivity. The increased channel numbers and tight structure increase the polarization sensitivity of AWG. Temperature interrogation experiments show that the FBG sensor interrogation is drastically affected when the effect of polarization sensitivity on the ultrasmall AWG is sufficiently large.

Keywords: Arrayed waveguide grating, Polarization, Silicon-On-Insulator, Fiber Bragg grating.

***Hongqiang Li, lihongqiang@tjpu.edu.cn

1 Introduction

Fiber Bragg grating (FBG) sensors have attracted increasing attention because they provide considerable advantages over conventional electrical sensors.[1–7] Several FBG sensor interrogation methods, such as dynamic matched grating filtering,[8] Fabry-Perot filter method,[9,10] Mach-Zehnder modulator method,[11,12] tunable narrow-line width laser scanning,[13] and arrayed waveguide grating (AWG) interrogation,[14,15] have been proposed. Among these FBG sensor interrogation methods, the dynamic matched grating filtering method exhibits the simplest structure and the lowest accuracy. The Fabry-Perot filter method possesses high resolution but requires complicated equipment. The Mach-Zehnder method cannot be used in quasistatic measurements. The tunable narrow-line width laser scanning method requires high amounts of light. The AWG-based FBG sensor interrogation system has attracted attention because of its high precision and high speed. However, traditional AWGs cannot satisfy the latest requirements for miniaturization given their large sizes.

Thus, a specially designed AWG with suitable size and performance for AWG interrogation must be developed.

A compact AWG can be fabricated on a silicon-on-insulator (SOI)-based platform because of its ultrahigh relative refractive index difference in the Si core and low-index claddings. These characteristics allow for sharp bends and enable size reduction to the micrometer, as well as the integration of scaled-up structures with other devices in a microsystem.[16] Therefore, SOI-based AWG miniaturization warrants further study. Yang proposed a 48×48 AWG on an SOI platform with 0.8 nm channel spacing. The fabricated AWG has a compact size of approximately $220\mu m \times 470\mu m$ and exhibits an insertion loss and a crosstalk of less than -4 and -15 dB, respectively.[17] Wang proposed an 8×8 silicon nanowire AWG that has a crosstalk of approximately -17 dB, an insertion loss of approximately -2.92 dB, and a footprint of only $730\mu m \times 300\mu m$.[18] Park fabricated an eight-channel AWG that demonstrates an insertion loss of 0.63 dB and a crosstalk of -23 dB to -25.3 dB.[19] Zou fabricated two SOI AWG routers that exhibit significantly improved spectral responses relative to those exhibited by SOI AWG routers with conventional design.[20] However, the effect of polarization sensitivity on ultrasmall SOI AWG for an FBG sensor interrogation system remains uninvestigated.

This study proposes a 1×8 SOI AWG, which possess core sizes of $350\mu m \times 250\mu m$. Simulation results show that these ultrasmall SOI AWGs exhibit large wavelength drift under transverse electric (TE) and transverse magnetic (TM) modes. The polarization sensitivity of the AWG increases because of the increase in channel number and tight structure. The experimental results show that the 1×8 AWG has an insertion loss of less than -3.4 dB, a crosstalk of less than -23.4 dB, and a channel spacing of 1.9 nm. Temperature interrogation experiments show that the proposed FBG sensor interrogation system that is based on the 1×8 AWG displays a high-interrogation

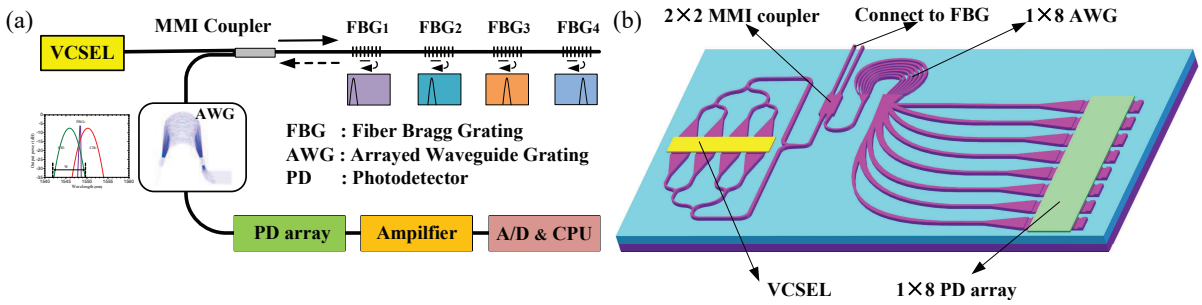

Fig 1 Schematic of the proposed FBG sensor interrogation system. (a) Schematic of the AWG interrogation of FBG sensors. (b) Hybrid Si photonic chip for the proposed FBG sensor interrogator system.

accuracy over the range of 10 $^{\circ}C$ to 50 $^{\circ}C$ and temperature measurement errors of less than 0.3 $^{\circ}C$.

2 Principle, design and analysis

The proposed FBG sensor interrogation system consists of a light source, a 2×2 multimode interference coupler,[21] 1×N/2 FBG distributed sensors, a 1×N SOI AWG,[22] a 1×N photodetector array,[23] subsequent signal amplification circuits, an analog-to-digital converter, and a data processing unit (Fig. 1 (a)). The light from the light source penetrates the FBG through the coupler. The reflected light also penetrates the AWG through the coupler. In case of interference from other AWG channels, the central wavelength of each FBG must be in the middle of the central wavelengths of two adjacent AWG channels. When the related variables that affect the spectrum of FBG change, the spectrum will shift and its overlap changes with each AWG channel, thus changing the light intensity in each channel. Each adjacent AWG channel can be used to demodulate variables. SOI is a well-known microelectronics and optoelectronics platform. Extremely small devices can be fabricated on SOI substrates because of the ultrahigh refractive index between Si and SiO_2. A schematic of the hybrid silicon photonic chip for the proposed FBG sensor interrogator system is shown in Fig. 1 (b).

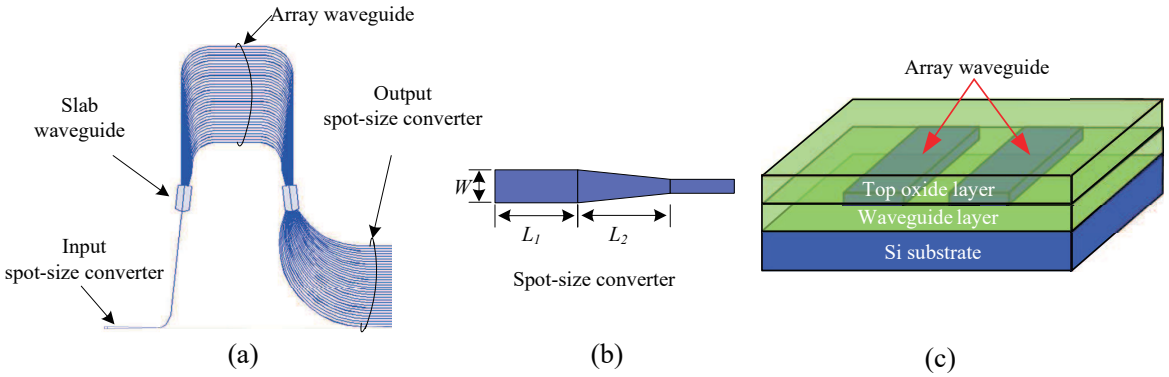

Fig 2 (a) AWG principle. (b) Structure of the spot-size converter. (c) Cross-sectional schematics of the arrayed waveguides of the AWG.

The $1 \times N$ AWG is the key component of the FBG sensor interrogation system. In this study, three types of ultrasmall $1 \times N$ SOI AWGs are designed. These AWGs consist of input, slab, array, and output waveguides, as shown in Fig. 2(a). Fig. 2(b) shows the structure of the spot-size converter. Light is launched into the planar waveguide through the input spot-size converter. The planar waveguide is designed in accordance with the Rowland circle principle, wherein it can diffract light in the arrayed waveguide. Each arrayed waveguide is located on a circle with its center located at the end of the center input waveguide. The diffracted light enters the arrayed waveguides in the same phase. Fig. 2(c) presents the cross-sectional schematics of the arrayed waveguides of the AWG. In the arrayed waveguides, a length difference (ΔL) is observed between adjacent waveguides. Thus, lights of different wavelengths can attain the same phase difference in the waveguide output. This phase difference results in wavelength-dependent wavefront tilting. The lights with different wavelengths will then focus on each output spot-size converter. Finally, the results of all output gratings are measured by a spectrometer, then a spectrogram is plotted. This spectrogram can be used to analyze the different types of AWG problems.

When light is transmitted in AWG, the different polarization states of the frequencies of the TE and TM modes shift because waveguide birefringence directly affects the performances of the

AWG devices. n_{TE} and n_{TM} are assumed to be the TE and TM modes of the effective index rate, respectively. The waveguide birefringence is thus $B = n_{TE} - n_{TM}$. The wavelength shift attributed to TE and TM modes is assumed to be $\Delta\lambda$. The center wavelength that corresponds to the polarization state is expressed as follows:

$$\lambda_{TM}(f) = c / f \; n_{TM}(f), \tag{1}$$

$$\lambda_{TE}(f) = c / f \; n_{TE}(f), \tag{2}$$

where f is the center frequency, and c is the light velocity. $\Delta\lambda$ is expressed as follows:

$$\Delta\lambda = cB \; / \; f \;\; n_{TE} n_{TM}, \tag{3}$$

W is the channel width of the $1 \times N$ AWGs. The increment in the channel width will affect the interrogation results because of the polarization effect. The interrogation results will be unaffected when the wavelength drift is less than the wavelength spacing of the AWG but will be seriously affected when $\Delta\lambda$ is large. The output wavelength shift of the AWG under TE and TM modes is shown in Fig. 3(a). Fig. 3(b) shows the schematic of the FBG-reflected wave in the measurement results of the $1 \times N$ AWG. When the channel width of the AWG is considerably large, a large channel crosstalk will occur, causing the reflected signals of the FBG to enter numerous channels. Thus, the temperature interrogation system will not work properly.

Different types of spot-size converters and AWGs are designed through the finite-difference time-domain (FDTD) method. The OptiFDTD simulation software is used for parameter opti-

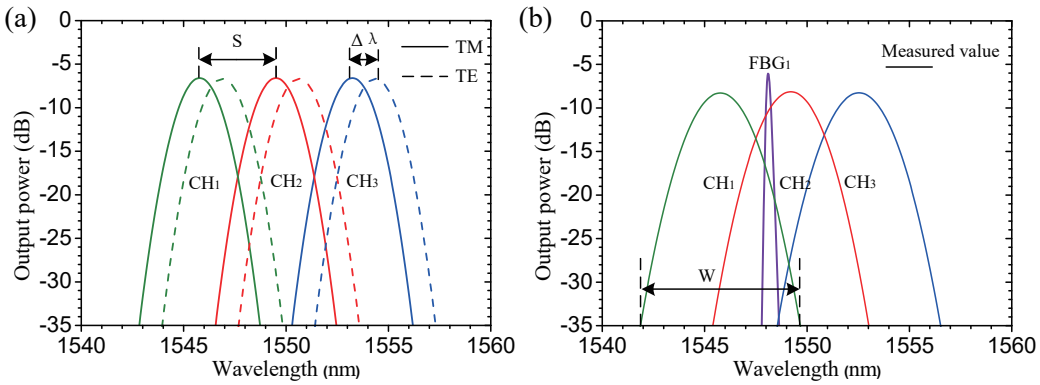

Fig 3 (a) Output wavelength shift diagram of AWG under TE and TM modes. (b) Schematic of FBG-reflected wave in the measurement results of the 1×N AWG.

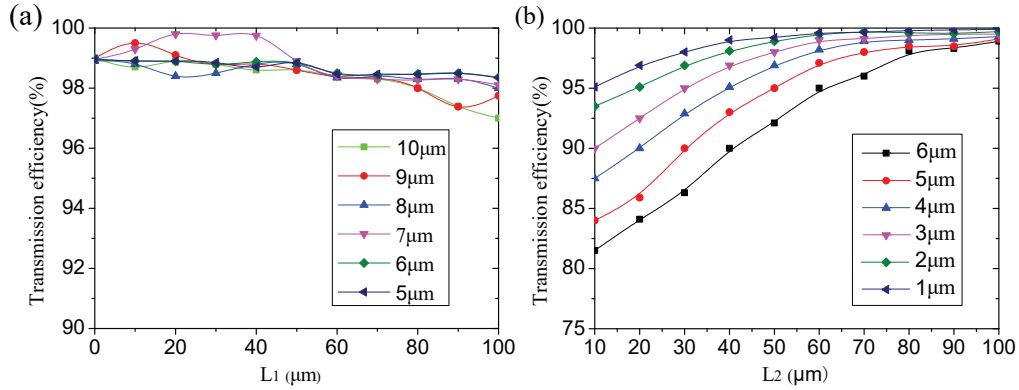

Fig 4 Simulation results for input spot-size converter with different parameters. (a) Transmission efficiency as a function of the input spot-size converter length of L_2 with different L_1 values. (b) Transmission efficiency as a function of the input spot-size converter length of L_2 with different Ws.

mization in the simulation experiment. The results show that the AWG with a $0.35\mu m$ waveguide width exhibits the best transmission spectrum. Fig. 4 presents the transmission efficiency of the input spot-size converter with different parameters. Fig. 4(a) depicts that the change in W minimally affects transmission efficiency. Moreover, the change in W negligibly affects transmission efficiency when L_2 is greater than $90\mu m$ (Fig 4 (b)). Under such results, the parameters of the input spot-size converter can be set as $W = 6\mu m$ and $L_2 = 95\mu m$.

The simulation results of the input spot-size converter are presented in Fig. 5(a), which shows that the insertion loss of the input spot-size converters is approximately less than -0.6 dB. The

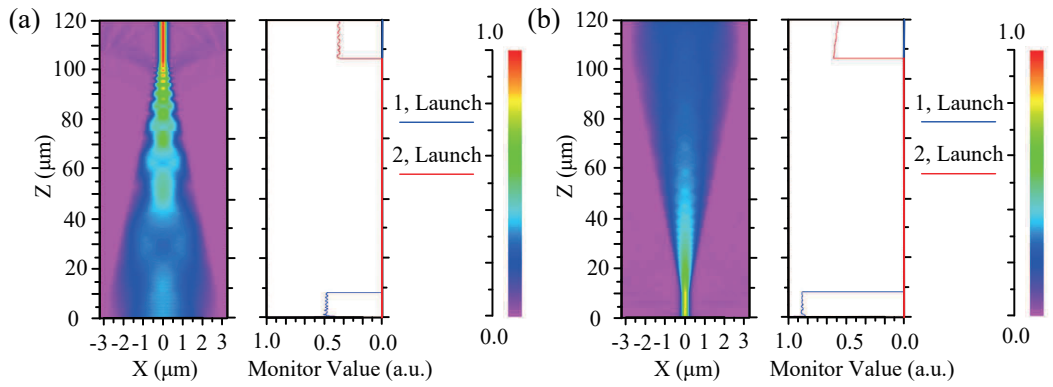

Fig 5 Simulation results of (a) input and (b) output spot-size converters. "1, Launch" and "2, Launch" represent the input light power of the spot-size converter, respectively.

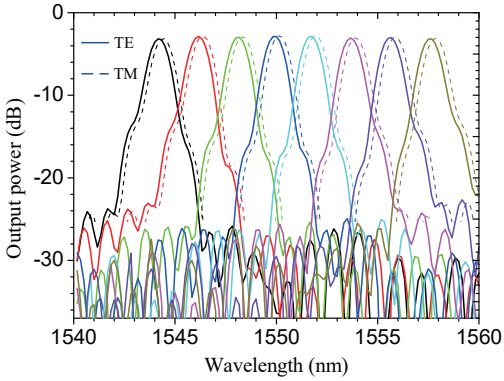

Fig 6 Simulation results of the 1×8 AWG with 30 arrayed waveguides.

same method is used to study the output spot-size converter. The simulation results of the output spot-size converter are presented in Fig. 5(b), which shows that the insertion loss of the output spot-size converters is approximately less than -1.3 dB.

In this study, the AWG structure is optimized by designing different waveguide widths and shapes to obtain the parameters for a high-performance AWG. A 1×8 AWG is designed with 30 arrayed waveguides and the core size of $350\mu m \times 250\mu m$. The arrayed waveguide width of all the AWGs is $0.35\mu m$. The simulation results show that the 1×8 AWG with 30 arrayed waveguides exhibits the best transmission spectra, with an insertion loss of less than -3.2 dB and a crosstalk of less than -23.7 dB, as shown in Fig. 6.

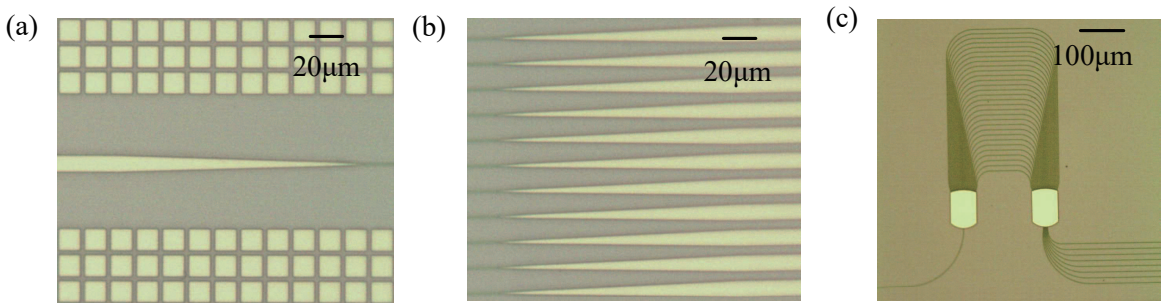

Fig 7 Schematic layout of the microscopy images of the (a) input spot-size converter, (b) output spot-size converter, and (c) 1×8 AWG with 30 arrayed waveguides (core size is 350 μm × 250 μm).

The simulation results of the three types of AWGs are presented in Table 1, which shows that the channel spacing and the wavelength drift of the 1×8 AWG are 1.9 and 0.3 nm, respectively. This wavelength drift is small relative to the wavelength spacing, thus implying that the 1×8 AWG displays high-resolution accuracy in temperature interrogation experiments.

Table 1 Simulation results of the 1×8 AWG.

Type	AWG core size(μm^2)	Insertion loss(dB)	Crosstalk (dB)	Wavelength range(nm)	Channel spacing(nm)	Wavelength drift(nm)
1×8	350×250	-3.2	-23.7	1543-1558	1.9	0.3

3 Experimental results of the optical elements

In reference to the comprehensively optimized design shown above, the designed AWGs and their photonic integrated system are fabricated on a standard SOI wafer with a 220 nm-thick top Si and a $2\mu m$-thick buried oxide. The AWGs are fabricated at the Institute of Microelectronics, Singapore via electron beam exposure and response-coupled plasma technology. The microscopy images of the local parts of the spot-size converter are shown in Figs. 7(a) and 7(b). All of the AWGs have the same input and output spot-size converters. Figs. 7(c) shows the microscopy images of the 1×8 AWG.

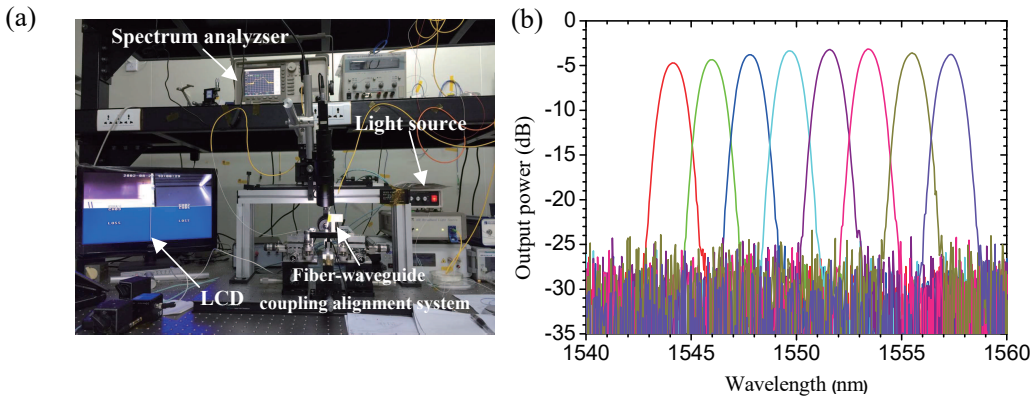

Fig 8 Experimental results. (a) Optical experimental setup consisting of a light source, tapered lensed single-mode fibers, a fiber–waveguide coupling alignment system, and a spectrum analyzer. (b) Experimental results obtained with the 1×8 AWG with 30 arrayed waveguides.

The experiment is performed by using the optical experimental setup shown in Fig. 8 (a). The optical experimental setup includes a light source (10 mW SLED, 1550 nm wavelength), tapered lensed single-mode fibers (2 m long, 900 μm Hytrel loose-tube buffered fibre, 7 mm stripped length, $2 \pm 0.5\mu m$ spot diameter, and $12 \pm 3\mu$ m working distance), a fiber-waveguide coupling alignment system ($\pm$0.1 dB alignment accuracy, $\pm$0.1 dB/h stability, ≤ 0.5 μ m gap accuracy, and 1 time W.D. 68 mm LED light), and a spectrum analyzer (-70 dBm sensitivity, 0.050 nm resolution). The tapered lensed single-mode fibers are used to connect the SOI devices and spectrum analyzer. The fiber-waveguide coupling alignment system is used to align the optical fiber and Si waveguide. The experimental results show that the insertion loss of the input spot-size converter is -0.9 dB, whereas that of the output spot-size converter is -1.7 dB. The input and output waveguide width of the AWG is $0.35\mu m$, and the waveguide spacing is $1\mu m$. The 1×8 AWG with 30 arrayed waveguides exhibits an insertion loss of -3.4 dB, a crosstalk of less than -23.4 dB, and a channel spacing of 1.9 nm, as shown in Fig. 8 (b).

4 Interrogation experimental results and discussion

In the FBG sensor interrogation experiments, when the reflection light of FBG penetrates the AWG, light with a different wavelength separates and travels to different adjacent array waveguides. When each FBG reflection spectrum passes through the adjacent channel of the AWG, the reflection spectrum overlaps with the transmission spectrum of two AWG adjacent channels. P_i and P_{i+1} are the two adjacent channels of the output light intensity of AWG. Additionally, P_i and P_{i+1} are the convolutions of the FBG reflection spectrum and the AWG adjacent channel transmission spectrum, respectively. P_i and P_{i+1} are expressed as follows:

$$\boldsymbol{P}_i = (1 - L_i) \int_0^\infty S(\lambda) \cdot R_{FBG}(\lambda) \cdot T_{AWG}(i, \lambda) d\lambda \,, \tag{4}$$

$$\boldsymbol{P}_{i+1} = (1 - L_{i+1}) \int_0^\infty S(\lambda) \cdot R_{FBG}(\lambda) \cdot T_{AWG}(i+1, \lambda) d\lambda \,, \tag{5}$$

where $S(\lambda)$ is the output power spectrum of the light source with the assumption that the output power is constant S_0 within the AWG bandwidth. L_i and L_{i+1} are the light attenuation coefficients. $R_{FBG}(\lambda)$ is the reflection spectrum function of the sensory grating. $T_{AWG}(i, \lambda)$ and $T_{AWG}(i+1, \lambda)$ are the AWG channels, and i and i+1 are the transmission spectrum functions in the fiber grating interrogation system. The relationship between the adjacent channel light intensity ratio logarithm of AWG and that of the FBG central wavelength is written as follows:

$$\ln(\frac{P_{i+1}}{P_i}) = \frac{8(\ln 2)\Delta\lambda}{\Delta\lambda_i^2 + \Delta\lambda_{FBG}^2} \lambda_{FBG} - \frac{4(\ln 2)(\lambda_{i+1}^2 - \lambda_i^2)}{\Delta\lambda_i^2 + \Delta\lambda_{FBG}^2} \,, \tag{6}$$

where $\Delta\lambda$ is the adjacent two-channel central wavelength difference in AWG at the initial

temperature. When FBG is subjected to constant stress, λ_{FBG} exhibits a linear relationship with temperature. Temperature change can be measured in real time by measuring the dual-channel light intensity and by calculating the logarithm of light intensity ratio.

In the FBG sensor interrogation experiment involving the 1×8 AWG, the central wavelengths of the FBG sensors are 1544.75, 1549.05, 1552.25, and 1556.35 nm. The bandwidths are less than 0.25 nm. These experimental results indicate a Bragg wavelength shift of approximately 10 pm/$^{\circ}C$ against temperature change over the tested wavelength range. The wavelength spacing of the AWG is less than 1.9 nm, indicating that the range of the Bragg wavelength shift cannot exceed 1.9 nm. The wavelength drift ranges of the four AWGs are less than 0.8 nm, indicating that the measurable range is less than 80 $^{\circ}C$, as shown in Fig. 9(a). However, the measurement range of the FBG sensor interrogation system is limited because of some reasons. In the temperature interrogation experiment, FBG sensors are placed on a temperature control platform. The actual temperature is the temperature of the temperature control platform, and the measured temperature is the temperature measured by the FBG sensor interrogation system. The experimental results show that the FBG sensor interrogation system displays high accuracy at 10 $^{\circ}C$ to 50 $^{\circ}C$. Fig. 9(b) shows the wavelength drift of the four FBGs at different temperatures. Fig. 9(c) shows the relationship between the measured and actual temperatures of one FBG sensor. The errors for all measured and actual temperatures are less than 0.3 $^{\circ}C$.

Table 2 Experimental results of the 1×8 AWG.

Type	AWG core size(μm^2)	Insertion loss(dB)	Crosstalk(dB)	Channel width(nm)
1×8	350×250	-3.4	-23.4	2.8

The optimization scheme for the FBG sensor system has two directions. The first direction involves the optimization of device performance to improve system performance. Future work

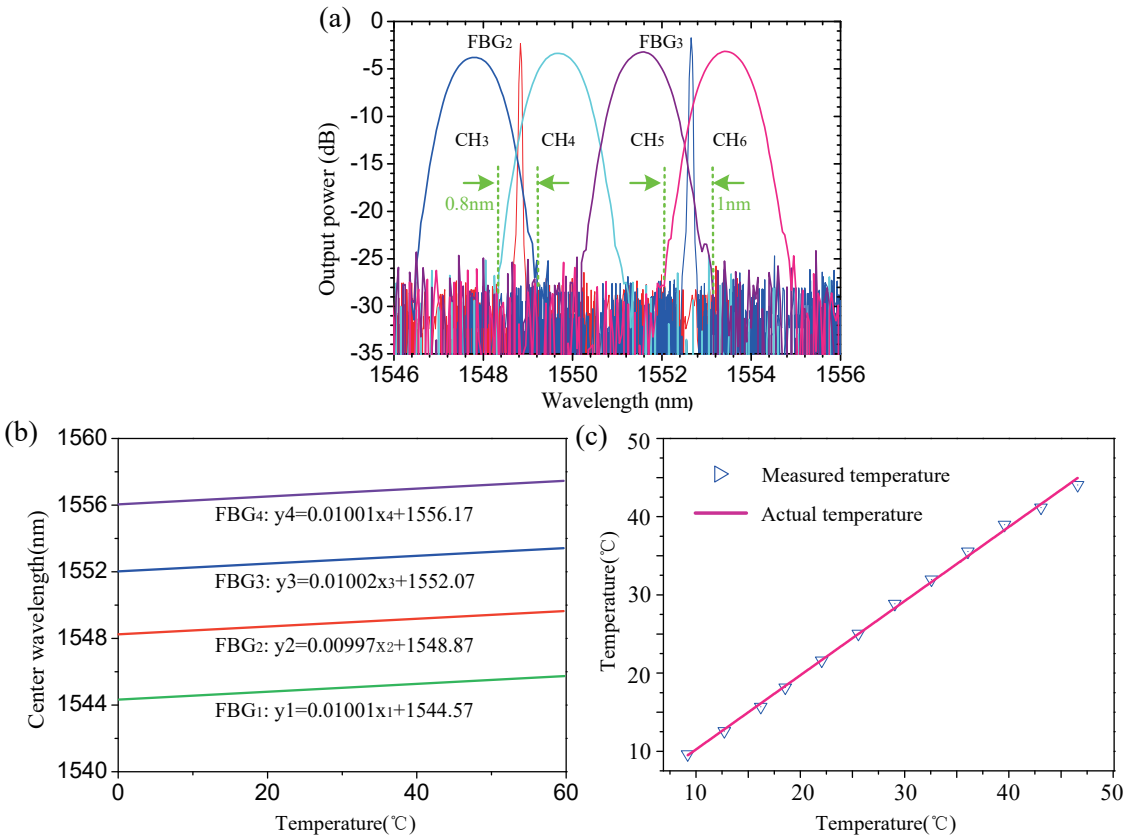

Fig 9 (a) Reflected wave of FBG in different channels of 1×8 AWG with 30 arrayed waveguides $(CH_3 - CH_6)$. (b) Wavelength drift of the four FBGs at different temperatures. (c) Relationship between the measured and actual temperatures.

will focus on improving device performance to reduce insertion loss and channel crosstalk. The other scheme is the optimization of the demodulation algorithm used in tracking wavelength shifts in FBGs. The optimized algorithm should be more accurate and faster than other well-known demodulation algorithms.

5 Conclusion

An SOI-based AWG is proposed in this study. The core sizes of the proposed AWG are smaller than $530\mu m \times 480\mu m$. The simulation results show that the wavelength drifts of the 1×8 AWG is 0.3 nm under TE and TM modes. The polarization sensitivity of the AWG increases because of the increase in channels and tight structure. The experimental results of the optical elements show that

the 1×8 AWG provides an insertion loss of less than -3.4 dB, crosstalk of less than -23.4 dB, and channel spacing of 1.9 nm. The results of the temperature interrogation experiment show that the FBG sensor interrogation system based on the 1×8 AWG displays high interrogation accuracy at 10 $^{\circ}C$ to 50 $^{\circ}C$. Errors in the measured and actual temperatures are lower than 0.3 $^{\circ}C$. The results of this study, which investigates the polarization sensitivity of ultrasmall $1 \times N$ SOI AWG, will serve as important references for future works on FBG sensor interrogation.

Acknowledgments

This work was supported by the National Natural Science Foundation of China (grant no. 61711530652, 61675154, 61504093, 61177078), and Sêr Cymru National Research Network in Advanced Engineering and Materials.

References

1 G. Rodriguez, M. Jaime, F. Balakirev, *et al.*, "Coherent pulse interrogation system for fiber bragg grating sensing of strain and pressure in dynamic extremes of materials," *Opt. Express* **23**(11), 14219–14233 (2015).

2 G. Woyessa, K. Nielsen, A. Stefani, *et al.*, "Temperature insensitive hysteresis free highly sensitive polymer optical fiber bragg grating humidity sensor," *Opt. Express* **24**(2), 1206–1213 (2016).

3 S. Kim, "Effect of sensing distance of aluminum-coated fbg sensors installed on a composite plate under a low-velocity impact," *Compos. Struct.* **160**, 248–255 (2017).

4 S. Zheng, B. Shan, M. Ghandehari, *et al.*, "Sensitivity characterization of cladding modes in long-period gratings photonic crystal fiber for structural health monitoring," *Measurement* **72**, 43–51 (2015).

5 S. Zheng, Y. Zhu, and S. Krishnaswamy, "Fiber humidity sensors with high sensitivity and selectivity based on interior nanofilm-coated photonic crystal fiber long-period gratings," *Sensor Actuat. B-Chemical* **176**, 264–274 (2013).

6 S. Zheng, M. Ghandehar, and J. Ou, "Photonic crystal fiber long-period grating absorption gas sensor based on a tunable erbium-doped fiber ring laser," *Sensor Actuat. B-Chemical* **223**, 324–332 (2016).

7 S. Zheng, "Long-period fiber grating moisture sensor with nano-structured coatings for structural health monitoring," *Struct. Health Monit.* **14**(2), 148–157 (2015).

8 J. Pan, J. Zhao, E. Li, *et al.*, "Optimization of dynamic matched grating filtering demodulation drived by piezoelectric ceramic," *Acta Photon. Sin.* **39**(2), 243–246 (2010).

9 H. Gao, S. Yuan, L. Bo, *et al.*, "Ingaas spectrometer and f-p filter combined fbg sensing multiplexing technique," *J. Lightwave Technol.* **26**(19), 2282–2285 (2010).

10 W. Huang, W. Zhang, T. Zhen, *et al.*, "A cross-correlation method in wavelet domain for demodulation of fbg-fp static-strain sensors," *IEEE Photon. Technol. Lett.* **26**(16), 1597–1600 (2014).

11 Y. Jiang, W. Ding, P. Liang, *et al.*, "Phase-shifted white-light interferometry for the absolute measurement of fiber optic mach-zehnder interferometers," *J. Lightwave Technol.* **28**(22), 3294–3299 (2010).

12 J. Zhou, L. Xia, R. Cheng, *et al.*, "Radio-frequency unbalanced m-z interferometer for wavelength interrogation of fiber bragg grating sensors," *Opt. Lett.* **41**(2), 313–316 (2016).

13 L. S. Yan, A. Yi, W. Pan, *et al.*, "A simple demodulation method for fbg temperature sen-

sors using a narrow band wavelength tunable dfb laser," *IEEE Photon. Technol. Lett.* **22**(18), 1391–1393 (2010).

14 J. Koch, M. Angelmahr, and W. Schade, "Arrayed waveguide grating interrogator for fiber bragg grating sensors: measurement and simulation," *Appl. Opt.* **51**(31), 7718–7723 (2012).

15 B. Shen, P. Wang, R. Polson, *et al.*, "An integrated-nanophotonics polarization beamsplitter with 2.4×2.4 μm_2 footprint," *Nat. Photon.* **9**, 378–382 (2015).

16 S. Pathak, E. Lambert, P. Dumon, *et al.*, "Compact soi-based awg with flattened spectral response using mmi," in *2011 IEEE 8th International Conference on Group IV Photonics (GFP)*, *IEEE Proc. GFC* **8**, 45–47 (2011). [doi:10.1109/GROUP4.2011.6053710].

17 B. Yang, Zhu, Y. Zhu, *et al.*, "Compact arrayed waveguide grating devices based on small su-8 strip waveguides," *J. Lightwave Technol.* **29**(13), 2009–2014 (2011).

18 J. Wang, Z. Sheng, L. Li, *et al.*, "Low-loss and low-crosstalk 8×8 silicon nanowire awg routers fabricated with cmos technology," *Opt. Express* **22**(8), 9395–9403 (2014).

19 J. Park, G. Kim, H. Park, *et al.*, "Performance improvement in silicon arrayed waveguide grating by suppression of scattering near the boundary of a star coupler," *Appl. Optics* **54**(17), 5597–5602 (2015).

20 J. Zou, Z. Le, J. Hu, *et al.*, "Performance improvement for silicon-based arrayed waveguide grating router," *Opt. Express* **25**(9), 9963–9973 (2017).

21 H. Li, X. Dong, E. li, *et al.*, "Design optimization and comparative analysis of silicon-nanowire-based couplers," *IEEE Photonics J.* **4**(5), 2017–2026 (2012).

22 H. Li, E. Li, Z. Liu, *et al.*, "Design of 1×8 si nanowire awg for on-chip awg demodulation integration microsystem," *Opt. Eng.* **51**(12), 123001–123005 (2012).

23 H. Li, B. Cui, Y. Liu, *et al.*, "Investigation of the chip to photodetector coupler with subwavelength grating on soi," *Opt. Laser Technol.* **76**, 79–84 (2016).

Hongqiang Li is currently a professor in school of electronics and information engineering at Tianjin Polytechnic University, China, and performs research activity at Tianjin Key Laboratory of Optoelectronic Detection Technology and Systems, China. He has published more than 130 journal and conference papers. His current research interests include fiber Bragg grating sensors, interrogation system and silicon-based photonic integration.

List of Figures

List of Tables